Epitaxial Electrodeposition of Zinc Oxide Nanopillars on Single-Crystal Gold

Run Liu, Alexey A. Vertegel, Eric W. Bohannan, Thomas A. Sorenson, and Jay A. Switzer*

Department of Chemistry and Graduate Center for Materials Research, University of Missouri−Rolla, Rolla, Missouri 65409-1170

Received September 21, 2000. Revised Manuscript Received December 2, 2000

ZnO nanopillars have been electrodeposited epitaxially onto Au(111), Au(110) and Au(100) single-crystal substrates. The nanopillars grow with the same [0001] out-of-plane orientation on all three substrates. The in-plane orientation was probed by X-ray pole figure analysis. The pole figures had six peaks on Au(111) and twelve peaks on Au(110) and Au(100). Scanning electron microscopy revealed aligned hexagonal nanopillars of ZnO with an average grain size of 85 nm on Au(111). There were two sets of hexagonal grains with an average size of 85 nm on Au(110) and 95 nm on Au(100) that were rotated 90° with respect to each other. Rocking curve analysis showed that the ZnO on Au(100) had the smallest mosaic spread.

Introduction

Zinc oxide is a large band gap (3.3−3.6 eV) *n*-type semiconductor which is of interest for high-frequency piezoelectric resonators, conducting transparent windows for photovoltaic cells, and UV light-emitting devices. The growth of epitaxial films of ZnO onto hexagonal substrates such as sapphire by vapor deposition techniques has been well-documented.[1−6] Electrodeposition of ZnO films has been demonstrated by Lincot and Peulon[7−8] and by Izaki and Omi.[9−10] Penner and co-workers synthesized ZnO nanoparticles and films using a hybrid electrochemical/chemical (E/C) method.[11] Searson and Wong fabricated thin films of quantum-size ZnO particles by electrophoretic deposition from stable colloidal suspensions.[12] Recently, Pauporte and Lincot have shown that epitaxial films of ZnO can be electrodeposited onto single-crystal gallium nitride.[13] In their work, both the film and substrate have a hexagonal structure and the lattice mismatch is only 2.4%.

Although studies on epitaxy have traditionally focused on systems with low lattice mismatch, there is increasing interest in the epitaxial growth of strained systems with large mismatch. Low mismatch systems are ideal for growing layered structures such as superlattices, but large mismatch systems can be used to produce ordered three-dimensional structures. In the Stranski−Krastanov (SK) model for high mismatch systems, the films grow initially as strained two-dimensional films, but then relax by island formation after a critical thickness. A system that has received much attention in this area is Ge films on single-crystal Si.[14−18] The lattice mismatch in this system is 4.2%. The films grow two-dimensionally for 3−8 monolayers, after which they relax to form self-assembled, quantum dots of nanocrystalline islands.

Our interest is in epitaxial systems with large mismatch. We have previously shown that epitaxial films of δ-Bi_2O_3,[19] Cu_2O,[20] PbS,[21] PbS/Cu_2O heterojunctions,[22] Tl_2O_3,[23] and Fe_3O_4[24] can be electrodeposited onto single-crystal gold substrates. Here, we show that epitaxial nanopillars of hexagonal ZnO can be electrodeposited onto cubic Au(111), Au(110), and Au(100) single-crystal substrates. Zinc oxide has the wurtzite crystal structure with $P6_3mc$ space group and lattice parameters $a = b$

* E-mail: jswitzer@umr.edu.

(1) Vispute, R. D.; Talyansky, V.; Trajanovic, Z.; Choopun, S.; Downes, M.; Sharma, R. P.; Venkatesan, T.; Woods, M. C.; Lareau, R. T.; Iliadis, A. A. *Appl. Phys. Lett.* **1997**, *70*, 2735.
(2) Kang, H.; Nakamura, K.; Lim, S.; Shindo, D. *Jpn. J. Appl. Phys.* **1998,** *37*, 781.
(3) Doh, S. J.; Park, S. I.; Chou, T. S.; Je, J. H. *J. Vac. Sci. Technol., A.* **1999,** *17*, 3003.
(4) Craciun, V.; Elders, J.; Gardeniers, J. G. E.; Boyd, I. W. *Appl. Phys. Lett.* **1994**, *65*, 2963.
(5) Fons, P.; Iwata, K.; Niki, S.; Yamada, A.; Matsubara, K. *J. Cryst. Growth* **1999**, *201/202*, 627.
(6) Tavernier, P. R.; Verghese, P. M.; Clarke, D. R. *Appl. Phys. Lett.* **1999**, *74*, 2678.
(7) Peulon, S.; Lincot, D. *Adv. Mater.* **1996**, *8*, 166.
(8) Peulon, S.; Lincot, D. *J. Electrochem. Soc.* **1998**, *145*, 864.
(9) Izaki, M.; Omi, T. *Appl. Phys. Lett.* **1996**, *68*, 2439.
(10) Izaki, M.; Omi, T. *J. Electrochem. Soc.* **1996**, *143*, L53.
(11) Nyffenegger, R. M.; Craft, B.; Shaaban, M.; Gorer, S.; Erley, G.; Penner, R. M. *Chem. Mater.* **1998**, *10*, 1120.
(12) Wong, E. M.; Searson, P. C. *Appl. Phys. Lett.* **1999**, *74*, 2939.
(13) Pauporte, Th.; Lincot, D. *Appl. Phys. Lett.* **1999**, *75*, 3817.
(14) Williams, R. S.; Medeiros-Ribeiro, G.; Kamins, T. I.; Ohlberg, D. A. A. *Acc. Chem. Res.* **1999**, *32*, 425.
(15) Ross, F. M.; Tromp, R. M.; Reuter, M. C. *Science* **1999**, *286*, 1931.
(16) Lagally, M. G.; Zhang, Z. *Science* **1997**, *276*, 377.
(17) Lagally, M. G.; Qin, X. R. *Science* **1997**, *278*, 1444.
(18) Lagally, M. G.; Liu, F.; Wu, F. *Chem. Rev.* **1997**, *97*, 1045.
(19) Switzer, J. A.; Shumsky, M. G.; Bohannan, E. W. *Science* **1999**, *284***,** 293.
(20) Bohannan, E. W.; Shumsky, M. G.; Switzer, J. A. *Chem. Mater.* **1999**, *11*, 2289.
(21) Vertegel, A. A.; Shumsky, M. G.; Switzer, J. A. *Angew. Chem., Int. Ed.* **1999**, *38*, 3169.
(22) Vertegel, A. A.; Shumsky, M. G.; Switzer, J. A. *Chem. Mater.* **2000**, *12*, 596.
(23) Vertegel, A. A.; Shumsky, M. G.; Switzer, J. A. *Electrochim. Acta* **2000**, *38*, 3233.
(24) Nikiforov, M. P.; Vertegel, A. A.; Shumsky, M. G.; Switzer, J. A. *Adv. Mater.* **2000**, *12*, 1351.

10.1021/cm000763l CCC: $20.00
Published on Web 01/06/2001

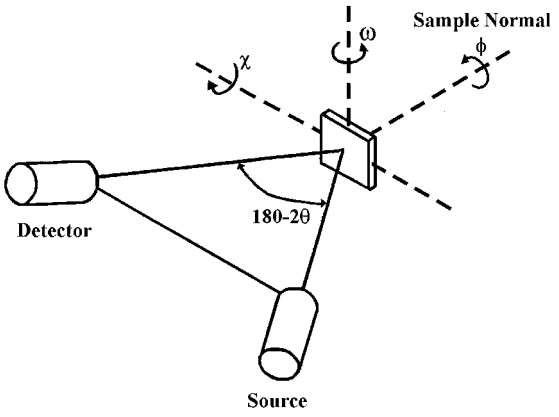

Figure 1. Schematic of the experimental setup used to determine the in- and out-of-plane orientations of epitaxial films by X-ray diffraction. The out-of-plane orientation is determined in the Bragg−Brentano configuration by standard $\theta-\theta$ scans. The out-of-plane mosaicity is determined by rocking the sample about the ω-axis. Rotating the sample 360° about the ϕ-axis results in a two-dimensional azimuthal scan. Constructing azimuthal scans for a series of tilt angles, χ, results in a three-dimensional pole figure, in which the epitaxy of the film has been determined for all crystallographic planes of the substrate.

$= 0.3250$ nm and $c = 0.5207$ nm. Gold has the cubic close-packed metal crystal structure with space group $Fm3m$ and $a = 0.4079$ nm. The lattice mismatch in this system calculated from $(a_{ZnO} - a_{Au})/a_{Au}$ is −20.3%.

Experimental Section

ZnO was deposited using the method developed by Lincot and Peulon.[7,8] The deposition solution contained 2×10^{-3} M $ZnCl_2$, and the supporting electrolyte was 0.1 M KCl. Water was HPLC-grade (Aldrich), and all other chemicals were reagent-grade (Aldrich). The temperature of the deposition bath was 65 °C, and oxygen gas (99.99%) was bubbled through the solution during the deposition. Working electrodes consisted of 1 cm diameter Au(100), Au(110), and Au(111) single crystals purchased from Monocrystals company, and Au(111) on mica substrates from Molecular Imaging. A gold wire fitted around the edge of the single crystals served as the electrical contact during deposition. The counter electrode was a platinum wire. The deposition was performed at a fixed potential of −0.7 V with respect to the SCE reference electrode with an EG&G Princeton Applied Research model 273A potentiostat/galvanostat. The thickness of the deposit was varied from 10 to 1000 nm depending on the deposition time. The critical factors to grow ZnO films are the temperature of the solution and the concentration of $ZnCl_2$. The temperature should be above 50 °C, and the concentration of $ZnCl_2$ should be below 1×10^{-2} M.

X-ray diffraction (XRD) experiments were performed with a Scintag 2000 diffractometer with a texture goniometer using Cu Kα radiation. Micrographs of the deposited films were obtained with a Hitachi model S4700 cold field emission scanning electron microscope.

Results and Discussion

The out-of-plane orientation and in-plane orientation of the films were determined by X-ray diffraction using the Bragg (θ), rocking (ω), tilt (χ), and azimuthal (ϕ) angles shown in Figure 1. The out-of-plane orientation was determined in the Bragg−Brentano configuration by standard $\theta-\theta$ scans with no tilt of the sample. The out-of-plane mosaicity was determined by rocking the sample about the ω axis. Evidence for in-plane texture

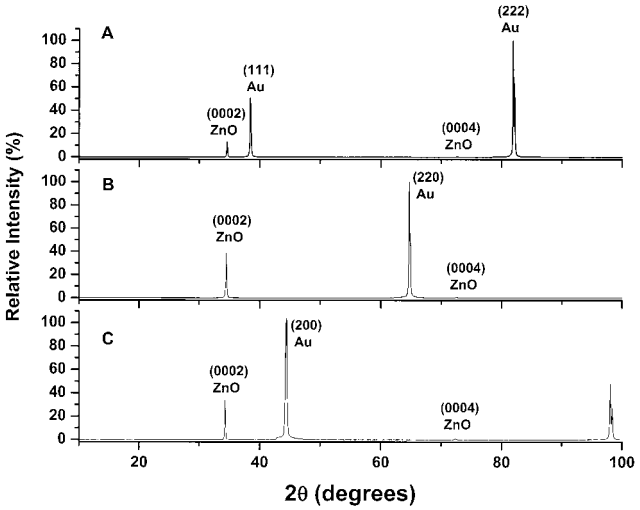

Figure 2. 2θ X-ray patterns for 500-nm-thick ZnO films deposited onto (A) Au(111), (B) Au(110), and (C) Au(100) single-crystal substrates. Only the (0002) and (0004) reflections for the ZnO deposit are observed.

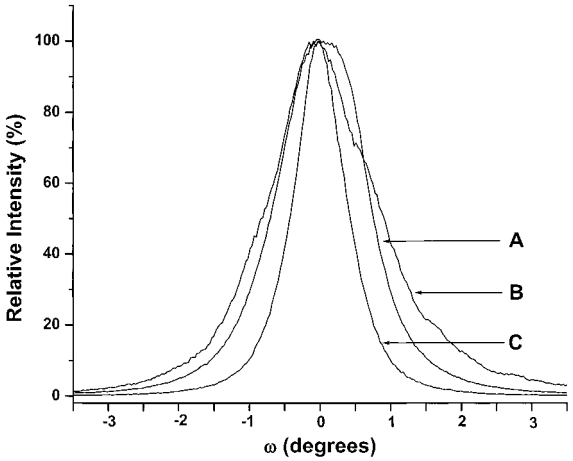

Figure 3. X-ray rocking curves for ZnO(0002) on (A) Au(111), (B) Au(110), and (C) Au(100) single-crystal substrates. The ZnO film on the Au(100) substrate had the smallest mosaic spread (0.87°).

was obtained by analysis of pole figures. The in-plane orientation of the film relative to the substrate was also determined. Pole figures were generated by tilting the sample over a range of tilt angles, and rotating the sample azimuthally at each tilt angle. Planes ($h'k'l'$) other than those parallel with the surface (hkl) are interrogated by selecting the Bragg angle for plane ($h'k'l'$). These planes satisfy the Bragg condition when the tilt angle, χ, corresponds to the angle between the (hkl) and ($h'k'l'$) planes. For example, the angle between the $(10\bar{1}1)$ and (0001) planes in a hexagonal system is 61.6°, and the angles between the (110) and (111) planes and the (100) and (111) planes in a cubic system are 35.3° and 54.7°, respectively.

Bragg−Brentano plots of the intensity versus 2θ for ZnO deposited onto the (111), (110), and (100) surfaces of Au are shown in Figure 2. Only the (0002) and (0004) peaks of ZnO are observed for all substrates, indicating a strong [0001] out-of-plane orientation of the ZnO. Rocking curves of the (0002) peaks of the ZnO on all of the substrates are shown in Figure 3. The full width at half-maximum (fwhm) values of the (0002) peaks of ZnO are 0.87° on Au(100), 1.72° on Au(110), and 1.45° on Au-

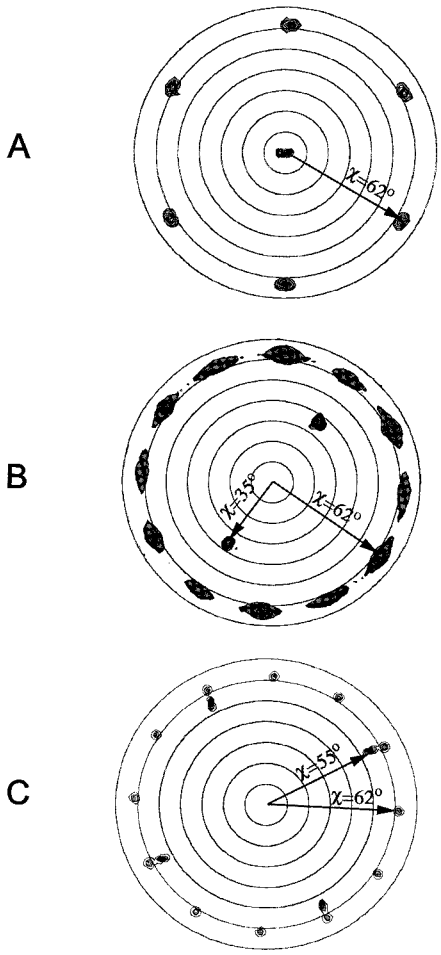

Figure 4. $(10\bar{1}1)$ X-ray pole figures for ZnO deposited onto (A) Au(111), (B) Au(110), and (C) Au(100) single-crystal substrates. The pole figures were obtained by setting 2θ equal to the angle of maximum diffracted intensity for the $(10\bar{1}1)$ planes ($2\theta = 36.16°$) and performing azimuthal scans at tilt angles, χ, from 0 to 70°. The pole figure for ZnO deposited on Au(111) has the expected 6-fold symmetry, and those of ZnO deposited on Au(110) and Au(100) have 12 peaks at $\chi = 62^o$. Since the ZnO $(10\bar{1}1)$ ($2\theta = 36.16°$) peak is close to the Au(111) ($2\theta = 38.18°$) peak, the substrate peaks appeared on the pole figures: one peak at $\chi = 0^o$ on Au(111), two peaks at $\chi = 35^o$ on Au(110), and four peaks at $\chi = 55^o$ on Au(100).

(111). The substrate fwhm values are 0.75° for the (200) reflection on Au(100), 0.77° for the (220) refection on Au(110), and 0.37° for the (111) reflection on Au(111). The ZnO film on the Au(100) substrate had the smallest mosaic spread, with a fwhm for the film (0.87°) that was only slightly larger than that of the substrate (0.75°).

Figure 4 shows the $(10\bar{1}1)$ plane pole figures for ZnO on Au(111), Au(110), and Au(100). The pole figure for the film deposited on Au(111) has six peaks at the expected tilt angle, χ, of 62°. The pole figure for ZnO deposited on Au(110) has 12 peaks. Six of the 12 peaks have a higher intensity than the other 6 peaks. On the basis of the substrate peaks at $\chi = 35^o$, we know that the more intense peaks are rotated 90° with respect to the substrate. The ZnO deposited on Au(100) also has 12 peaks, indicating that there are two in-plane orientations with a 90° rotation with respect to each other.

Epitaxial relationships that are consistent with the above experimental results are shown in Figure 5. The

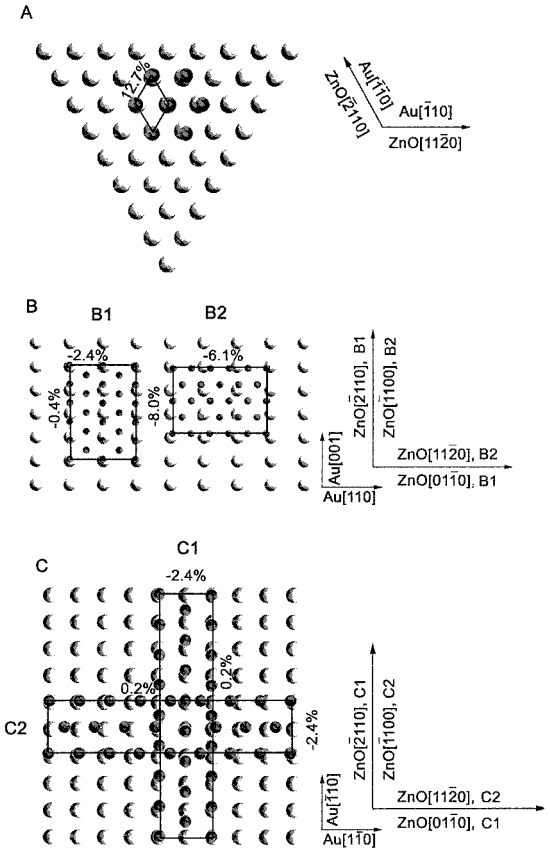

Figure 5. Epitaxial relationships for growth of ZnO on (A) Au(111), (B) Au(110), and (C) Au(100). The Au substrate atoms are light and the Zn atoms of ZnO are dark. The (1×1)Au-$(111)[\bar{1}10]$//(1×1)ZnO$(0001)[11\bar{2}0]$ coincidence lattice in part A has a mismatch of 12.7%. The coincidence lattice (4×2)-Au$(110)[001]$//(5×2)ZnO$(0001)[\bar{2}110]$ in part B1 has a mismatch of −0.4% along the Au[001] and ZnO$[\bar{2}110]$ directions and a mismatch of −2.4% along the Au[110] and ZnO$[01\bar{1}0]$ directions. The coincidence lattice (3×3)Au$(110)[110]$//(2×5)ZnO$(0001)[11\bar{2}0]$ in part B2 has a mismatch of −6.1% along the Au[110] and ZnO$[11\bar{2}0]$ directions and a mismatch of −8.0% along the Au[001] and ZnO$[\bar{1}100]$ directions. The coincidence lattice (9×2)Au$(100)[\bar{1}10]$//(8×1)ZnO$(0001)[\bar{2}110]$ in part C1 has a mismatch of 0.2% along the Au$[\bar{1}10]$ and ZnO-$[\bar{2}110]$ directions and −2.4% along the Au$[1\bar{1}0]$ and ZnO$[01\bar{1}0]$ directions. The coincidence lattice (2×9)Au$(100)[1\bar{1}0]$//(1×8)ZnO$(0001)[11\bar{2}0]$ in part C2 has a mismatch of 0.2% along the Au$[1\bar{1}0]$ and ZnO$[11\bar{2}0]$ directions and a mismatch of −2.4% along the Au$[\bar{1}10]$ and ZnO$[\bar{1}100]$ directions.

simpler model is that of ZnO(0001) on the Au(111) surface (Figure 5A). It is seen that the hexagonal Zn plane of ZnO is matched to the close-packed Au plane of Au(111). The in-plane epitaxial relationship is (1×1)Au$(111)[\bar{1}10]$//(1×1)ZnO$(0001)[11\bar{2}0]$ and the mismatch is 12.7%. The interface models of ZnO(0001) on Au(110) are shown in Figure 5B. There are two sets of in-plane epitaxial relationships which are marked as B1 and B2. The (4×2)Au$(110)[001]$//(5×2)ZnO(0001)-$[\bar{2}110]$ coincidence lattice in Figure 5B1 is rotated 90° with respect to the substrate. The mismatch along the Au[001] and ZnO$[\bar{2}110]$ directions is −0.4%, and that along the Au[110] and ZnO$[01\bar{1}0]$ directions is −2.4%. The (3×3)Au$(110)[110]$//(2×5)ZnO$(0001)[11\bar{2}0]$ coincidence lattice in Figure 5B2 is not rotated with respect to the substrate. The mismatch along the Au[110] and ZnO$[11\bar{2}0]$ directions is −6.1%, and the mismatch along the Au[001] and ZnO$[\bar{1}100]$ directions is −8.0%. The

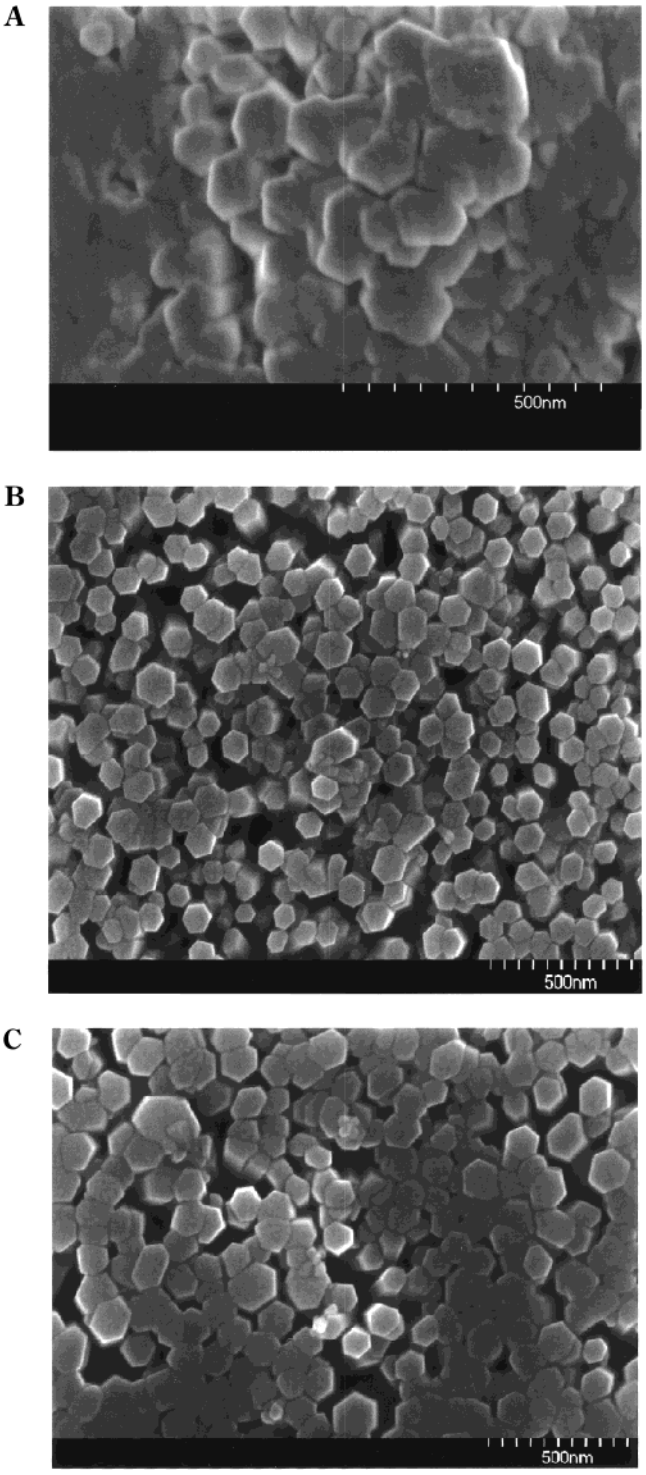

Figure 6. SEM micrographs of 500-nm-thick ZnO on (A) Au(111), (B) Au(110), and (C) Au(100). The hexagonal pillars have an average size of about 85 nm aligned with each other on the surface of the film on Au(111). Two kinds of hexagonal pillars with a 90° rotation are observed on the ZnO deposited on Au(110) and Au(100). In the case of Au(110), one type of the hexagonal pillars is dominant which is in agreement with the X-ray pole figures. The average grain size is about 85 nm on Au(110) and 95 nm on Au(100).

mismatch in Figure 5B2 is larger than that in the Figure 5B1. This is in agreement with the X-ray pole figure result which showed that the set of six peaks rotated 90° with respect to the substrate was dominant. The interface models are shown in Figure 5C for the Au(100) surface. There are two degenerate

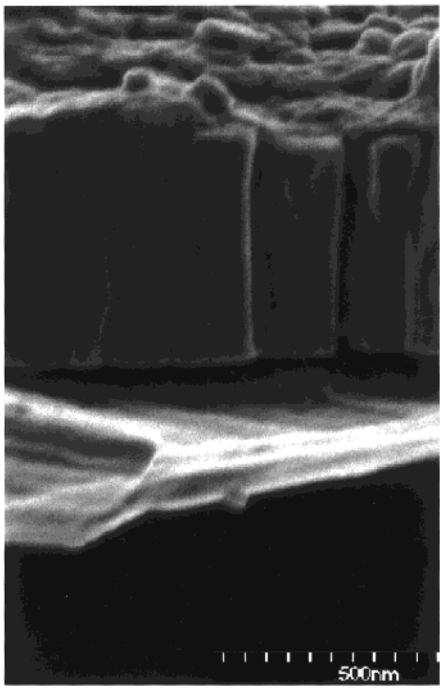

Figure 7. Cross-sectional SEM micrograph of ZnO on a Au(111)//mica substrate. The ZnO on this substrate has an out-of-plane and in-plane orientation determined by XRD. The film has a columnar microstructure with nanopillars that are about 500 nm high.

epitaxial relationships rotated 90° with respect to each other which are marked as C1 and C2. The coincidence lattices are (9×2)Au(100)[$\bar{1}$10]//(8×1)ZnO-(0001)[$\bar{2}$110] and (2×9)Au(100)[1$\bar{1}$0]//(1×8)ZnO(0001)-[11$\bar{2}$0]. The mismatch for the epitaxial relationship in Figure 5C1 along the ZnO[$\bar{2}$110] and Au[$\bar{1}$10] directions is 0.2%, and the mismatch along the ZnO [01$\bar{1}$0] and Au [1$\bar{1}$0] directions is −2.4%. The mismatch for the epitaxial relationship in Figure 5C2 along the ZnO[11$\bar{2}$0] and Au[1$\bar{1}$0] directions is 0.2%, and the mismatch along the ZnO[$\bar{1}$100] and Au[$\bar{1}$10] directions is −2.4%.

SEM micrographs of the samples are shown in Figures 6. Aligned hexagonal nanopillars were observed on the surface of the ZnO on Au(111). Two kinds of hexagonal nanopillars with a 90° rotation with respect to each other are observed on the ZnO deposited on Au(110) and Au(100). One type of hexagonal nanopillars is dominant on the Au(110) substrate, consistent with the X-ray pole figure. The grain size of the hexagonal pillars was approximately 85 nm on Au(111), 85 nm on Au(110), and 95 nm on Au(100). The height of the pillars was about 500 nm on all substrates. The diameter of the hexagonal nanopillars changes little with increasing thickness of the deposit. An SEM micrograph of a cross-section of ZnO grown on a Au(111)//mica substrate is shown in Figure 7. The SEM cross section reveals a columnar microstructure, which is consistent with the [0001] orientation observed by XRD. The mechanism of growth of the ZnO nanopillars is presently under study by analysis of current−voltage curves following a potential step. Initial results suggest that the growth does not occur by the Stranski−Krastanov mode, but that the nanopillars nucleate directly on the single-crystal gold.

Conclusions

The ZnO nanopillars in this study were *c* axis oriented, and had in-plane alignment on all surfaces of Au. The pillars had an average diameter of 85 nm on the Au(111) and Au(110) surfaces and 95 nm on the Au(100) surface. On the Au(111) surface, all pillars had the same in-plane alignment, whereas on the Au(110) and Au(100) surfaces, two in-plane orientations rotated 90° with respect to each other were observed. If these nanopillars are to be used as templates for molecular electronics or for data storage, it would be necessary for them to grow with some spatial order.[25,26] It would also be necessary to produced separated nanopillars. However, an application of these nanopillars in which spatial order would not be necessary would be as high-surface-area large band gap semiconductors for dye-sensitized photoelectrochemical cells. O'Regan et al. have produced efficient photoelectrochemical cells based on dye-sensitized nanoporous TiO_2[27] and ZnO.[28] Columnar ZnO nanopillars should provide more effective charge transport for the photogenerated carriers than that of particulate large band gap semiconductors.

Acknowledgment. Financial support by National Science Foundation Grants CHE-9816484, DMR-9704288, DMR-0071365, and DMR-0076338 is gratefully acknowledged.

CM000763L

(25) Kagan, C. R.; Mitzi, D. B.; Dimitrakopoulos, C. D. *Science* **1999**, *286*, 945.
(26) Collier, C. P.; Wong, E. W.; Belohradsky, M.; Raymo, F. M.; Stoddart, J. F.; Kuekes, P. J.; Williams, R. S.; Heath, J. R. *Science* **1999**, *285*, 391.
(27) O'Regan, B.; Grätzel, M. *Nature* **1991**, *353*, 737.
(28) O'Regan, B.; Schwartz, D. T.; Zakeeruddin, S. M.; Grätzel, M. *Adv. Mater.* **2000**, *12*, 1263.